

UNCLASSIFIED

Defense Technical Information Center
Compilation Part Notice

ADP014038

TITLE: Novel Microwave Photonic Techniques in the Future Military Systems

DISTRIBUTION: Approved for public release, distribution unlimited
Availability: Hard copy only.

This paper is part of the following report:

TITLE: Optics Microwave Interactions [Interactions entre optique et micro-ondes]

To order the complete compilation report, use: ADA415644

The component part is provided here to allow users access to individually authored sections of proceedings, annals, symposia, etc. However, the component should be considered within the context of the overall compilation report and not as a stand-alone technical report.

The following component part numbers comprise the compilation report:

ADP014029 thru ADP014039

UNCLASSIFIED

Novel Microwave Photonic Techniques in the Future Military Systems

Afshin S. Daryoush

Department of Electrical and Computer Engineering
Drexel University, Philadelphia, PA 19104, USA

Daryoush@ece.drexel.edu

Abstract

This paper reviews a number of novel applications of microwave photonic techniques in future military systems. One category is light interactions with microwave devices and circuits, which has contributed to the beginning of microwave photonics. The performance of HBT is the most attractive over FET and HEMT devices, due to its I-V dependence on high bandwidth and optical sensitivity. Moreover, different techniques of optical ADC are reviewed and among them all-optical ADC has the greatest promise of achieving high bit resolution. Microwave spectroscopy of biological tissues provides opportunity to create tomographic images of brain and breast, which leads to low-cost and reliable health monitoring of military personnel. A higher spatial resolution is obtained when a higher modulating frequency is employed. Finally, a new microchip laser is developed to generate frequency agile sources at microwave photonics. Optical sources operating at a fixed temperature will correspond to a beat signal, where a low phase noise beat signal is produced.

1. Introduction

In the last few years novel microwave photonics techniques are developed that lead to superior performance over purely electronic systems. Some examples of these techniques are reviewed that may form the basis of future robust military systems. The first approach is based on light interactions with microwave devices. A review of the previously established optically controlled devices and circuits are made and example of clock recovery circuit up to 100Gb/s is discussed. Next the concept of optical analog-to-digital converter is presented with capability of reaching 50 GSPS. Finally an approach based on diffused photon near infrared imaging technique is discussed leading to monitoring systems for pilot overload. As the modulation frequency expands in to upper microwave frequencies, spatial resolution increases. A microchip laser is presented which can be used as a chirped laser source with applications in lidar and medical imaging.

2. Light Interaction with Devices and Circuits

From early beginning of optical control of TRAPPAT and IMPATT in 1970, optical control of semiconductor devices has provided the promise of remote control along with isolation of optical source from other electrical sources. Over time a number of techniques have been developed to control performance of a number of devices and circuits using optical interactions. Various optically controlled microwave subsystems

have been demonstrated in the last twenty years, such as OCO and optically tuned filters [1], phase shifter [2], amplifiers [3], switches[4], and antennas [5]. Even though these techniques are intriguing, but have not found significant applications yet. More recently, spurred by rapid developments in fiberoptic based networks (MAN and LAN), the chip level integration of photonic and microwave components for high performance optical receivers have gained attention. PIN-amplifier configurations, such as PIN-HEMT [6] have been reported, and lately high performance PIN -HBT combinations have been realized by Aitken et. al. [7]. The three terminal microwave devices are attractive to perform photodetection and control functions in the receiver front-end [8, 9]. This configuration enhances receiver performance by reducing parasitics, requires less pre-amplification due to intrinsic gain of transistors, and has lower power consumption and less costly fabrication.

The key to these developments and related applications in communications and control of microwave systems is the understanding of the optical properties of microwave devices. Professors Seeds and Salles provided an excellent overview on this topic in 1990 [10]; however, since then the developments of HBT have brought more emphasis on the subject. Particularly photo-response of HBT, MESFET and HEMT could be unified and a comparison is made in terms of inherent photo-detection mechanism, gain, sensitivity, and bandwidth.

Static Analysis: Table I summarizes various effects that contributes to the photoresponse of the HBT, MESFET, HEMT, and its comparison to PIN photodiode. (The performance of PIN photodiode is considered as baseline.) For PIN photodiode the photoresponse current is determined by the photo-generated electron-holes pairs in the intrinsic region and no current gain is experienced. The light level directly controls the photocurrent in a linear fashion. On the other hand in HBT, in addition to photo-generated electrons at the collector depletion region, there is an increase in the effective base current due to the drift of photogenerated holes from the collector depletion region to the base. This source of this term is change in current injection rate due to change in base voltage and hence is labeled as internal photoconductive effect; since this increase occurs under constant bias current, it results in current gain. The photoresponse of the HBT is linear with optical power.

	I_{pvi}		I_{pvx}		I_{pc}		I_{pci}		I_{pd}	
PIN	----- -	-----	-----	-----	-----	-----	-----	-----	none	very fast
HBT	----- -	-----	-----	-----	-----	-----	moderate (linear)	fast	none	very fast
FET	large (log)	slow	large (log)	very slow	small	fast	-----	-----	-----	-----
HEMT	large (log)	slow	large (log)	very slow	small	fast	-----	-----	-----	-----

Table I . Sources of photo-detection mechanisms in popular microwave semiconductor transistors and their comparison to PIN photodiode as baseline.

On the other hand, the photoresponse in both field effect transistors (MESFET and HEMT) is attributed to three mechanisms [11]. The photogenerated carriers collected at the gate yield a photovoltage V_{phx} , when passing through an external resistor. Thus the *external photovoltaic* increases in gate bias, which opens the channel and results in a photocurrent of $I_{pvx} = g_m V_{phx}$. The *internal photovoltaic effect* results in $I_{pvi} = g_m V_{ph}$, where for MESFET [12] V_{ph} is a light-induced modulation of the channel height and in the case of the HEMT, V_{ph} represents a shift in the quasi-Fermi level [13]. The *photoconductive effects* I_{pc} are very small, and are neglected. The optical responsivity of microwave semiconductor transistors is compared in Fig. 1. At low illumination the logarithmic response of FET devices provides large gain. However, photoresponse saturates rapidly, which limits their dynamic range. The HBT, which has relatively large dark current, but low noise [14], performs best at moderate and high illuminations.

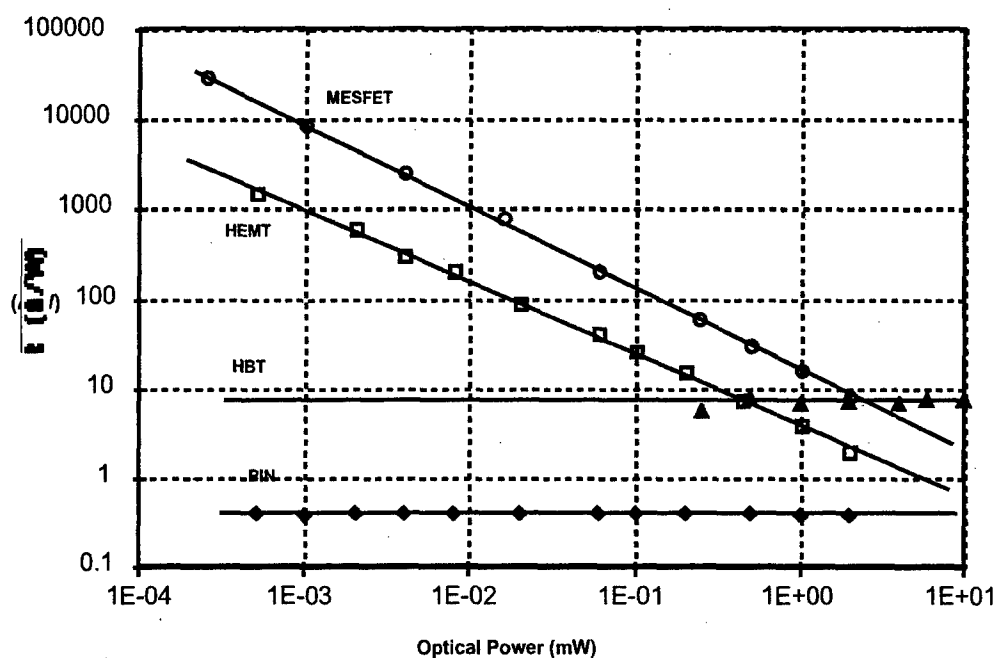


Fig. 2 Comparison of the static light responsivity for microwave transistors and their performance comparison to PIN Photodiode as a baseline. (Courtesy of Prof. P.R. Herzfeld of Drexel Univ.)

Dynamic Response: The frequency response of a PIN is limited by the carrier transit time, where a shorter intrinsic region yield a faster response but this behavior is at the expense of quantum efficiency for vertical devices. (Traveling wave photodiodes are designed to simultaneously meet high power handling, speed, and efficiency requirements.) The speed of the HBT is governed by sum of different time constants associated with the charging time of the B-E junction, the base transit time, the charging time of the B-C junction, and the transit time across the collector depletion region. The optical response of the HBT is fast since these time constants are the same as those which determine the HBT ultra high-speed response. Whereas for the FET devices the external photovoltaic effect is very slow because of the long charging time of the gate external circuit. The MESFET's dynamic response is dominated by the dynamics of the internal photovoltaic effect, which is defined by the RC time constant of substrate resistance and

the epi-layer/substrate junction capacitance [14]. For the HEMT, on the other hand, the RC time constant, determined by the buffer resistance and the change in electron concentration in the 2-DEG channel [12], defines the speed. It is important to note that the speed of photoresponse of the FETs is independent of their microwave speed.

The measured and calculated frequency response for these devices is depicted in Fig. 2. At low frequencies FETs perform well, but the intrinsically slow photovoltaic effect yields a small gain-bandwidth product. The speed of the HBT and PIN is comparable. Note, increasing the coupling efficiency of the HBT from 1% to 10%, which is a feasible task, will reduce the link insertion loss by 20dB, and thus supersedes that of the PIN. Using devices with larger β (e.g. 250 instead of 25) will also give additional advantage to the HBT.

Recent publication on nonlinear behavior of high-temperature superconducting film as photomixer has provided opportunity to generate THz signals using the kinetic inductive photoresponse [15]. These new applications maintain interest in light interaction with microwave circuits.

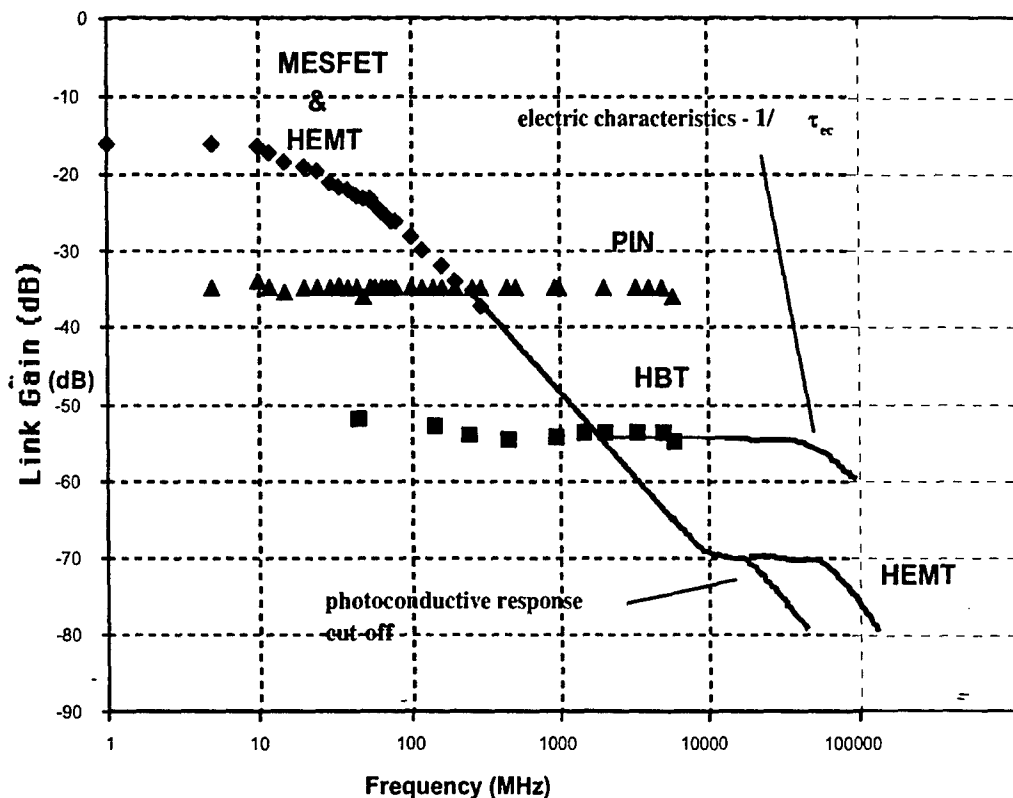


Fig. 2. Frequency response of microwave devices, measured data is represented by discrete points and theory by solid lines. The optical coupling efficiencies were calculated to be less than 1% for the HBT, 4% for the MESFET and the HEMT and 60% for the PIN. (Courtesy of Prof. P.R. Herczfeld of Drexel Univ.)

3. Optical ADC Techniques

Optoelectronic devices have demonstrated ultra-fast switching speed and mode-locked lasers have achieved high-speed and accurate optical pulses. With capability of sampling electrical signals at resolutions of sub-picoseconds, implementation of optical Analog-to-Digital Converter has long intrigued many researchers due to its following advantages. Since optical sampling has time jitter that is about 2 orders lower than electronic clock. Second, optical sampling decouples sampling electrical signal and sampled optical signals. Third, optical sampled or quantized signal is easy to distribute by fiber and remotely controlled. Also, many photonic ADC approaches also produce output as Gray-codes directly, eliminating the need for additional encoding circuits. However optical quantization is generally limited to resolution of a few bits and this remains a big challenge. There are two approaches to quantize the information after sampling by optical signal: i) hybrid optic-electronic ADC, where electrical quantizers are employed; and ii) all-optical ADC, where optical quantization is implemented.

Hybrid optic-electronic ADC: Hybrid optic-electronic ADC, or called optically assistant ADC, employs optical sampling followed by electronic quantization. It attempts to combine advantages of both optical and electronic ADC technologies: high-speed rate of optical sampling and high resolution of electronic quantization. But the speed of electronic devices is much lower than the optical sampling rate. So the sampled optical signal has to be down converted to lower speed and channeled to parallel electronic quantizers. For example, 100 GSPS sampled pulses can be split into 8 channels in time domain, and the pulse rate in every channel is 12.5 GSPS. Most optical sampling transducers are implemented with Mach-Zehnder modulators [16], where the output intensity of the Mach-Zehnder interferometer is function of the applied voltage:

$$I_{out} = I_i \cos^2\left(\frac{\varphi_0}{2} - \frac{\pi V}{2V_\pi}\right)$$

where $\varphi_0 = 2\pi nL/\lambda_0$, the optical distance of a branch, and V_π is the half-wave voltage, defined as the applied voltage at which the phase shift changes by π . Optical sampling operates in a small range around V_π , the output is approximately linearly proportional to applied voltage V . To extend the linear range of Mach-Zehnder modulator, a number of linearization approaches were demonstrated. In photonic ADC, the linearization can be implemented in digital domain by directly inverting the transfer function in DSP.

The key issue in hybrid opto-electronic ADC is to channelize high speed sampled optical pulses and ensure channels matching in amplitude and time. Based on approaches of channelization, three major schemes are proposed as: a) time interleaving [17], b) WDM channelized [18], c) time stretched [19]. The optical sampling and time interleaving is employed by Juodawlkis et al to implement an ADC with bandwidth up to 505 MSPS by using 1:8 optical demultiplexers and 14-bit electrical quantizers. A dual-output LiNbO₃ MZ modulator is used for linearization processing and a 65 dB SFDR and 47 dB SNR, corresponding to an effective resolution of 7.5 bits. The sampled optical pulses are split into 8 channels by optical time division demultiplexers, which are composed of 3 stages of 1×2 switches controlled by 505 MHz driving signals. Therefore the 16 parallel high-resolution electronic quantizers are working at 63 MSPS [18]. To achieve an interleaving SFDR of 80 dB, the converter-to-converter gains must be

matched to $\sim 0.01\%$, the offset must be matched to $\sim 0.01\%$ of the signal amplitude, and the converter-to-converter crosstalk must be less than one part in 10^4 .

On the other hand using optical dispersive components, multi-wavelength optical wave is smeared (for continuous spectrum) or split (for discrete wavelengths) in time, borrowing concept from WDM communication, the sampled optical signal can be channelized in both wavelength and time domains. The RF signal is sampled by the WDM pulses and then channelized by a WDM demultiplexer. Clark et al demonstrated a 100-GSPS photonic ADC based on the time- and wavelength-interleaved scheme [18] using mode-locked fiber laser (MLFL) that generates 12.5 GHz pulse train, and 100-GHz sampling optical pulses is obtained by an $8\times$ multiplexer. The pulses propagate through different fiber delays and attenuators which then are recombined in the WDM. The delay fibers and attenuators can be adjusted for time matching and amplitude equalizing respectively. The time interleaved pulse train is then demultiplexed into 8 channels according to wavelengths. The resulting parallel pulses are then to be quantized by >12.5 GSPS quantizers, but an 8-bit ADC operating at only 781 MSPS was achieved with SNR of 22~26 dB, which corresponds to about 4 bits. The resolution of wavelength channelized ADC is still limited since it faces similar difficulties as the time interleaving ADC does. The time uncertainty and amplitude uniformity between channels are difficult to control.

Bhushan et al demonstrated a record ultra-fast sampling rate of 130 GSPS using time stretching approach [19]. The idea behind this ADC is similar to wavelength channelized ADC, but in time stretched RF input signal modulates a broadband optical continuous wave (CW) other than is sampled by optical pulses with discrete wavelengths. The detected analog optical signal is sampled and quantized by electronic ADC. Fig. 3 shows a limited time application of time stretch preprocessing, where a passively mode-locked fiber laser with 20-MHz repetition rate followed by a 17 nm filter is used to generate broadband short pulses. The optical pulse propagates through a dispersive fiber of length L_1 and dispersed in time to get 0.8 ns time aperture. The wave is then modulated by RF signal to be converted. The modulated wave is sent to another piece of dispersive fiber of L_2 to be stretched in time domain. The ADC obtain a stretch ration of $M=16.2$ by proper choosing L_1 and L_2 , where then the stretched signal is detected and digitized by a single 8-GSPS electronic ADC of an oscilloscope. So the effective sampling rate is about 130 GSPS ($8\text{GSPS} \times 16.2$) with SNR of 45 dB, corresponding to 7.5 bits of resolution.

On the other hand for continuous signals in time, a parallel architecture must be used in order to preserve the information. In this process an arrayed waveguide grating (AWG) is employed to sample a portion of the optical spectrum and since each optical wavelength corresponds to a different propagation time delay, the filter performs sampling in time. Then each segment is time stretched by the same factor M prior to entering a slow electronic ADC, however both time alignment and amplitude in balance between various arms of are crucial.

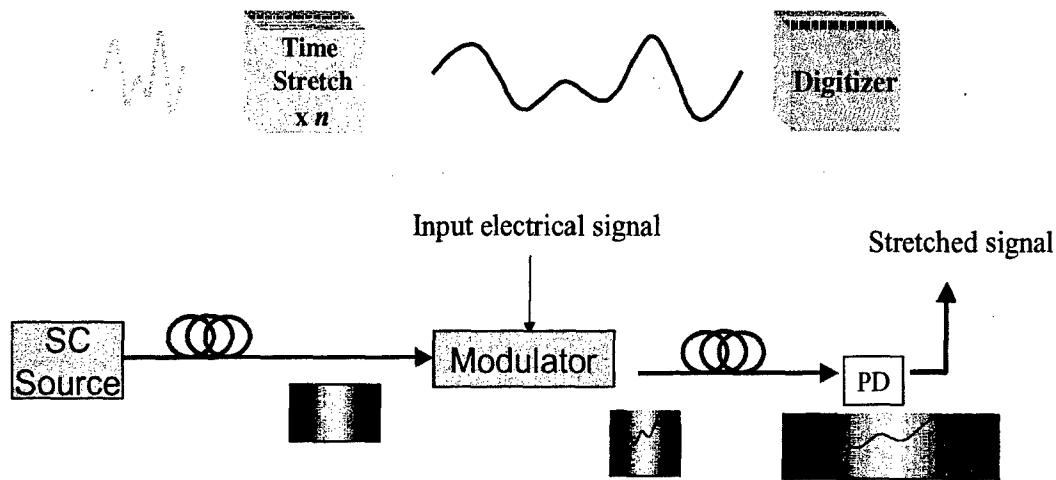


Fig. 3. Time limited signal converted by time stretching ADC [19]. (Courtesy of Prof. Jalali from UCLA)

All-optical ADC: There are quite a few ways to implement optical quantization, but probably the best known photonic ADC is based on by Taylor patent of 1977 [20]; a revised design called optical folding flash ADC in 1995 [21]. Fig. 4 shows a block diagram of a 4-bit optical folding-flash ADC. The geometrical scaling of V_π or electrode length is eliminated by a parallel-serial combined configuration. This scheme uses identical electrode length but sets DC bias at different points on the interferometer transfer characteristic curve. The resulting transfer function of MSB-2 and LSB branch is obtained by multiplying the functions of all stages at different bias and show doubled frequency comparing to previous bit. However this scheme also presents some additional challenges. First the MSB is susceptible to high noise because of the slow changing slope at digital edges. Second, the transit time limitation is still not eliminated; moreover, the hardware complexity increases exponentially in term of interferometer number as $2^{(b-1)}+1$ and it strongly relies on accurate bias.

Another way to quantize optical signal is to exploit variable electro-absorption semiconductor modulators demonstrated by Hayduk et al [22]. The quantization is achieved using an architecture that relates the

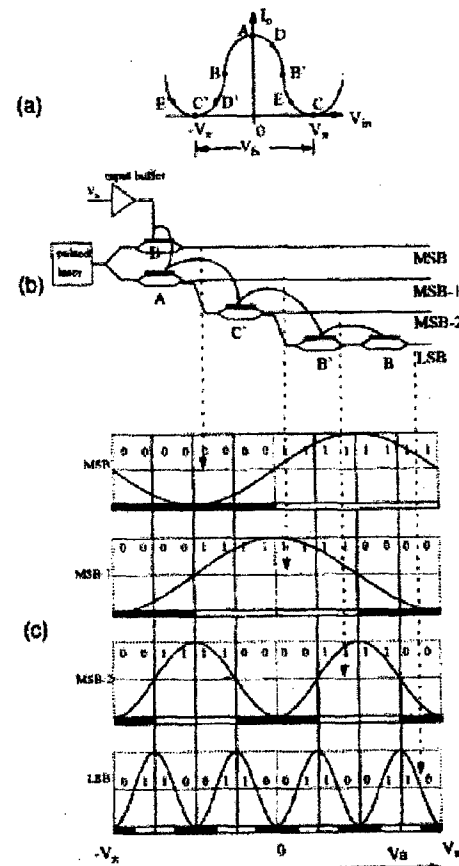


Fig. 4. Optical folding-flash ADC [21]. a) various bias points of all optical ADC, b) realization of MZ modulators for quantization, c) the received signal levels for each significant bit.

received analog voltage to an optical intensity, which shares the same idea with electronic flash ADC, in which 2^N-1 comparators with different threshold are used. The use of the passive materials in this flash photonic ADC architecture with no external voltage requirement makes this module very low power dissipation. The authors claim that the ADC has potential to operate at more than 100 GSPS combined with resolution as high as 12-14 bits. But this scheme is susceptible to amplitude fluctuation and unbalanced energy splitting. A similar idea is also employed in all-optical ADC quantization using photodetectors with different sensitivities [23].

In the two ADC schemes mentioned above, RF signal is sampled and quantized by optical amplitude. However the amplitude errors are strongly depends on source fluctuation, device linearity and loss along the optical link. So it is hard to build high resolution all-optical ADC based on optical amplitude. An all-optical ADC working in spectrum domain is demonstrated by Zmuda et al [24], as shown in Fig. 5. The input signal is sampled by a tunable laser and quantized by processor filters with binary behavior. The output wavelength of the tunable laser is modulated by the applied electrical field so the electrical amplitude is represented as wavelength in spectrum domain. The post-sampled light is processed by a parallel optical filter array. If the spectrum line falls into the pass band, the output is represented as "1", otherwise a "0" will be read. Each filter has periodic equally spaced passband and stopband and organized in a Gray code manner.

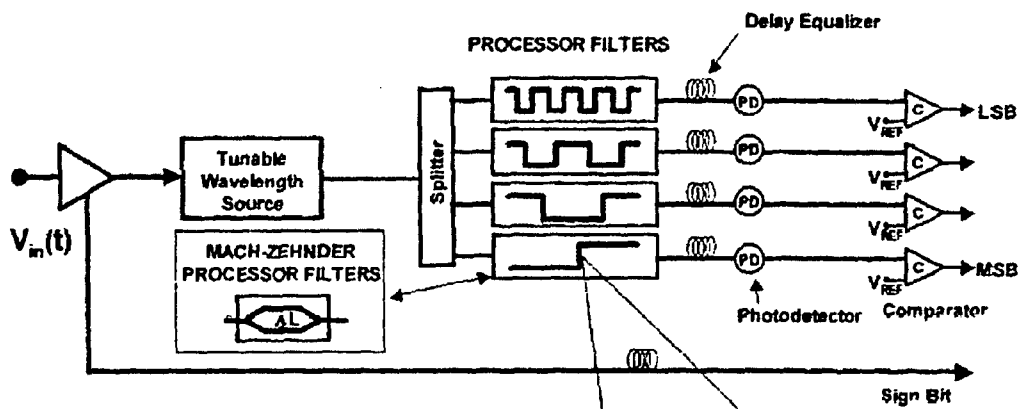


Fig. 5. Optical ADC using tunable laser and filters [24].

The major challenges for this scheme are the filter design of sharp transition and tunable laser. A 4-bit optical ADC using Bragg grating filters and ring cavity tunable laser is proposed and analyzed. Because of the convergence time limitation of Fabry-Perot cavity, only 4 bits of resolution can be achieved at 10 Gs/s. And the performance of Bragg grating filters (Fig. 6) show limited resolution. The authors proposed a folding circuit to enhance its resolution, where a Mach-Zehnder interferometer performs the optical folding circuit and first- or second-order linearization circuit corrects the nonlinear folded signal. So two low resolution ADCs are coupled with the folding circuit to achieve $M+N$ bits of resolution. The author claimed the ADC would be able to operate at conversion speeds in excess of 10 GHz with up to 10- to 12-bits of resolution. However, it is not clear how the upper M -bit ADC achieved the additional 6 to 8 bits. But it indicates a promising way to perform analog-to-digital in spectrum domain.

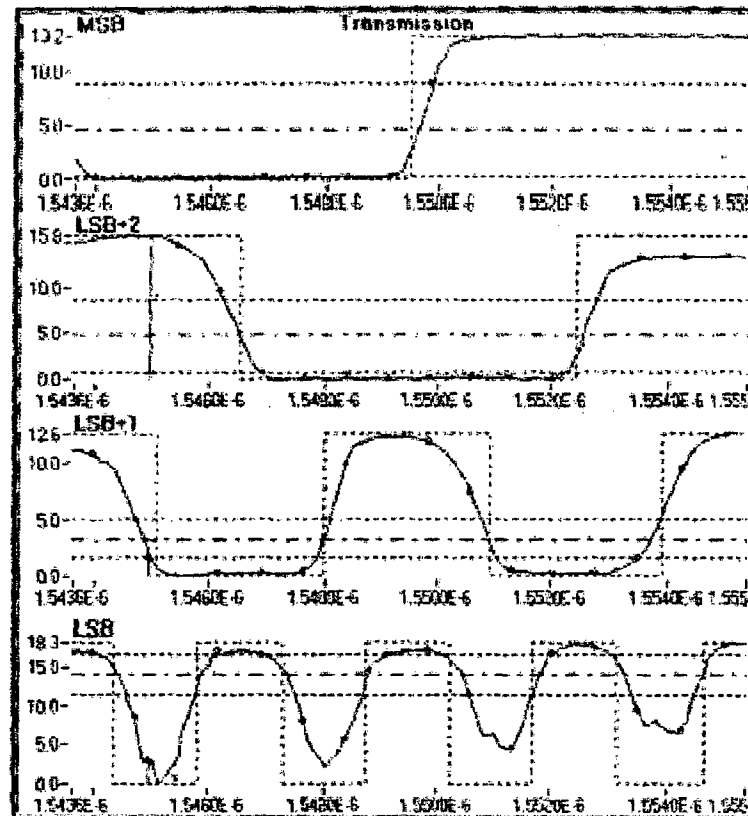


Fig. 6. Performance of Bragg grating filters [24].

4. Near IR Optical Spectroscopy

Near Infrared (NIR) spectroscopy is a new, non-invasive technique to analyze living tissue. In NIR spectroscopy, the main aim is to extract the optical properties (absorption and scattering) of the living tissue. Absorption information is used to characterize the concentration of biological chromophores, such as hemoglobin (in oxy and de-oxy forms), which in turn indicates the physiological changes in blood. This approach could be employed for health monitoring purposes, such as pilot overload in combat aircrafts. Scattering information provides information on composition, density, and organization of tissue structures, such as cells and sub-cellular organelles [25, 26]. Therefore, NIR techniques provide information about disease-related functional and structural changes. More specifically, it has been shown recently that physiological changes such as ischemia, necrosis and malignant transformation can produce

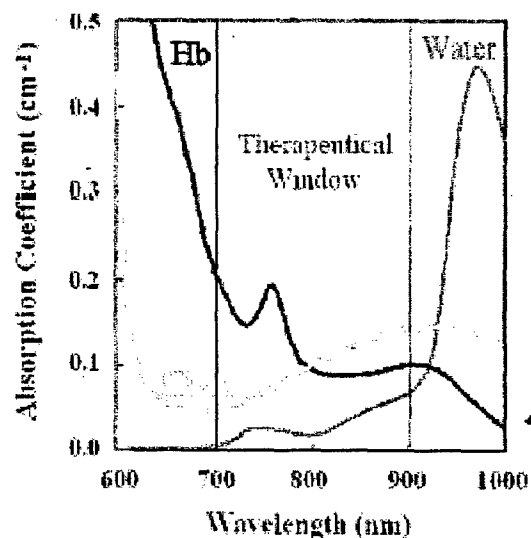


Fig. 7. Absorption spectrum of Hb (deoxy-hemoglobin), HbO₂ (oxy-hemoglobin), and water in the NIR region.

important perturbations in tissue optical properties [27]. The importance of NIR spectrum lies in the fact that in this region tissue absorption is much lower than the other parts of the spectra (see Fig.7). Apart from tissue information content, this region is attractive since NIR instruments are inexpensive to construct and are easily portable. These features allow NIR instruments to be an attractive alternative to other techniques, such as MRI. Moreover, NIR light is not an ionizing radiation; therefore, it can be used as a usual clinical monitoring of patients in radiation therapy.

The modulated NIR could be employed for greater spatial and temporal information and could be explained based on the following physical foundation. When photons enter a turbid (multiply scattering) media, the photons scatter randomly in all directions, diffuse through the medium, and get absorbed during this diffusion process. When source detector separation is large enough and scattering is dominating absorption, diffusion theory is very well suited approximation for photon transport:

$$\frac{1}{c} \frac{\partial \Phi(r,t)}{\partial t} - D \nabla^2 \Phi(r,t) + \mu_a \Phi(r,t) = S(r,t),$$

where Φ is the fluence rate (W/cm^2), c is the speed of light in the tissue, S is the source term, μ_a is the absorption, and D is the diffusion constant, which is related to reduced scattering constant, μ'_s , by $D = 1/(3 \cdot \mu'_s)$. In an infinite medium for a point source photon diffusion wave (PDW) can analytically be expressed as:

$$\Phi(r,t) = \frac{S}{4\pi D} \frac{\exp(ikr)}{r}$$

where k is the complex wave vector, (i.e., $k = k_{real} + ik_{imag}$) and is described as combination of modulating frequency, diffusion, and absorption coefficients as: $k = \sqrt{-\mu_a/D + i\omega/(c \cdot D)}$. The back-scattered PDW has phase lag and amplitude attenuation relative to the source as:

$$\Theta_{lag}(r, \omega) = k_{imag} \cdot r$$

$$A_{att}(r, \omega) = \exp(-k_{real}r) / (4\pi Dr)$$

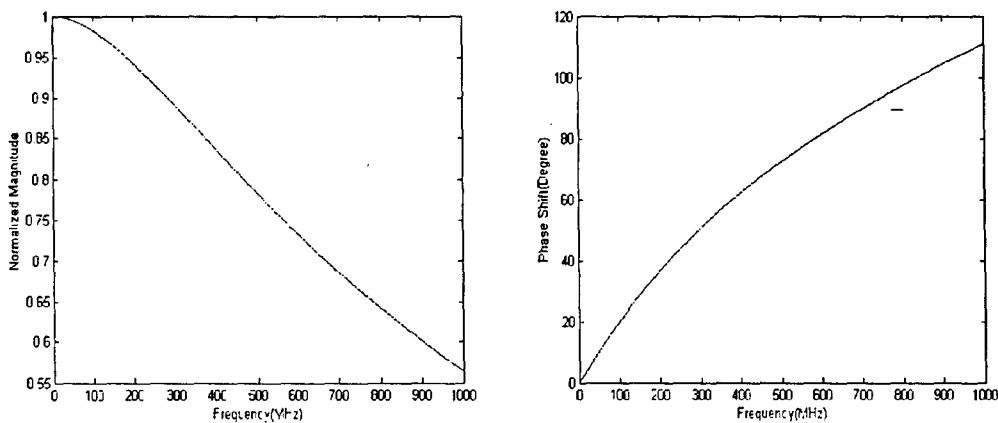


Fig. 8. Normalized amplitude attenuation (left) and phase-shift (right) of photon density waves as a function of frequency.

Fig. 8 shows the solution of amplitude attenuation and phase-shift of photon diffuse waves with respect to frequency (up to 1 GHz) for a breast tissue with optical absorption and scattering coefficients properties of $\mu_a = 0.05\text{cm}^{-1}$, $\mu'_s = 10\text{cm}^{-1}$. NIR techniques are also being used for brain imaging as seen in Fig. 9 [28, 29]. The image on the left is BOLD image from MRI. The image on the right is obtained from diffuse optical tomography.

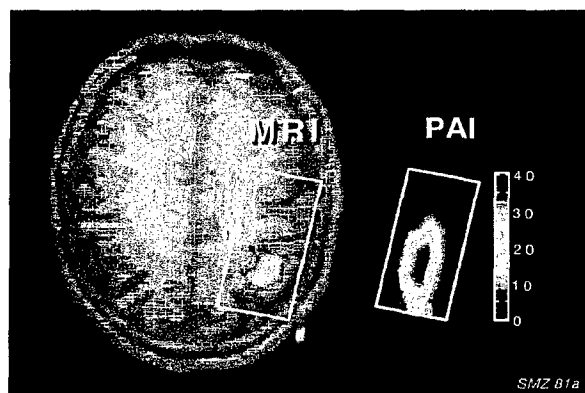


Fig. 9. Brain activation image. MRI image is shown on the left and the image from diffuse optical tomography is depicted on right. (Courtesy of Prof. Britton Chance of Univ. of Pennsylvania.)

NIR technique uses constant wave (CW), time-domain, and frequency domain instruments according to their applications and information content. The CW systems are very inexpensive, however suffers from limited resolution. Frequency domain instruments are more compact, cheaper, and algorithms are easier to handle than time-domain techniques, hence frequency-domain instruments are more attractive. In frequency-domain photon migration concept is easier too. When light is modulated with modulation frequencies in megahertz region, diffuse photon density waves (PDW) are generated, propagating with a wavelength of several centimeters [30-33]. At the detector one measures the amplitude decay and phase shift data of these waves (see Fig. 8). Amplitude and phase data are used to map the optical absorption and scattering properties of the medium. Optical constants in turn are used to obtain hemoglobin concentration, blood volume and oxygen saturation. More accuracy of the extracted results is achieved when a frequency swept mode is employed, and as the modulation frequency increases to microwave region a higher spatial resolution is attained.

5. Tunable Microchip Lasers

Compact, efficient solid-state microchip lasers, with high spectral quality, show great potential as optical transmitters for rapidly tunable sub-carrier sources in biomedical imaging and hybrid lidar-radar applications. Optical heterodyning of two ring-oscillators has been reported for millimeter-wave generation [34] using PZT tuning, which are essentially very slow processes. An alternative design topology is developed by Prof. P.R. Herzfeld and his group at Drexel University.

The basic microchip laser configuration is depicted in Fig.10, where two identical optical cavities are formed by depositing dielectric mirrors on opposite ends of a single

Nd:YVO₄/MgO:LiNbO₃ crystal assembly [35]. This configuration is comprised of a 0.3mm long Nd:YVO₄ crystal, which serves as the gain medium, and a 1.2 mm MgO:LiNbO₃ crystal, which is the tuning section. The two side-by-side lasers are pumped by an 808nm high power laser diode source. Electrodes are deposited on the top and the bottom of the 1.2 mm MgO:LiNbO₃ tuning section. The outputs of the two lasers are combined, coupled into a single mode fiber and transmitted to a high-speed optical detector. By applying an electrical field to one of the lasers, its refractive index is modulated, which modulates its lasing wavelength resulting at a millimeter wave signal. The difference in the optical wavelengths of two lasing sections, $\Delta\lambda_{opt}$, leads to the millimeter wave beat frequency, $f_{mm} = c \Delta\lambda_{opt} / \lambda_{opt}^2$. The monolithic configuration gives the device simplicity, compactness, stability, and reduced sensitivity to external temperature fluctuations. The actual device, mounted on a brass fixture, is depicted in Fig. 11.

The measured laser output power vs. pump power characteristic is depicted in Fig. 12. The threshold pump power is found to be 160mW, and the overall efficiency at 250mw pump power is approximately 12%. The frequency shift of the laser output as a function of temperature is shown in Fig. 13. From this measurement a temperature sensitivity of about 4GHz/°C is measured. Considering the monolithic configuration of the device, it is expected that two laser sections are at the same temperature, and temperature drift will affect both sections similarly. Realization of two laser sections in a single crystal assembly dramatically improves the temperature stability. By varying pump current, the crystal temperature or the applied electric field the beat frequency can be tuned from DC to 90 GHz. The optical spectrum of the two laser outputs is depicted in Fig. 14. To obtain this spectrum first the two lasers are adjusted so that their lasing frequencies were identical, then one of the lasers was tuned until the peak optical powers of the two lasers were 0.3 nm apart, which corresponds to 90 GHz beat frequency.

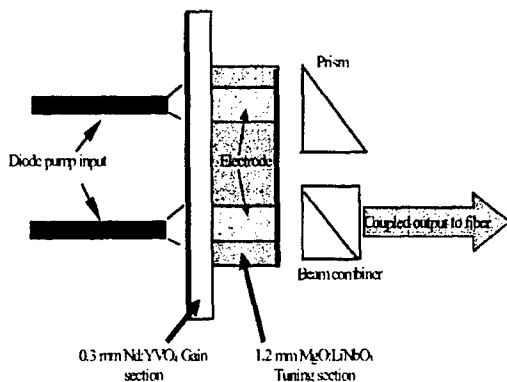


Fig. 10. The monolithic microchip laser structure [35].

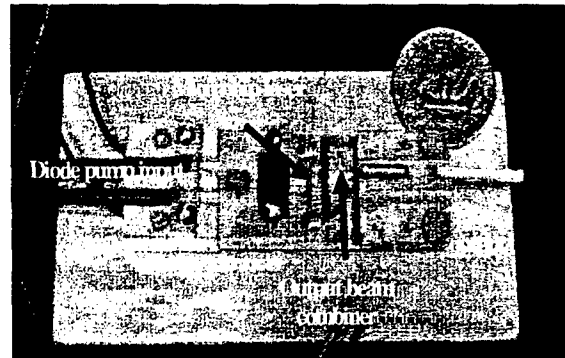


Fig.11. Picture of the heterodyne transmitter [35].

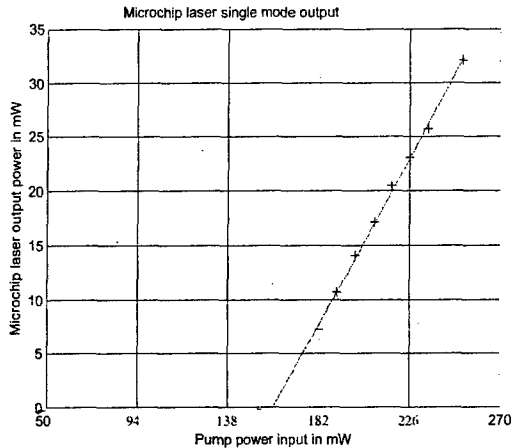


Fig. 12. The laser output power characteristics. The measured threshold pump power is 160mW [35].

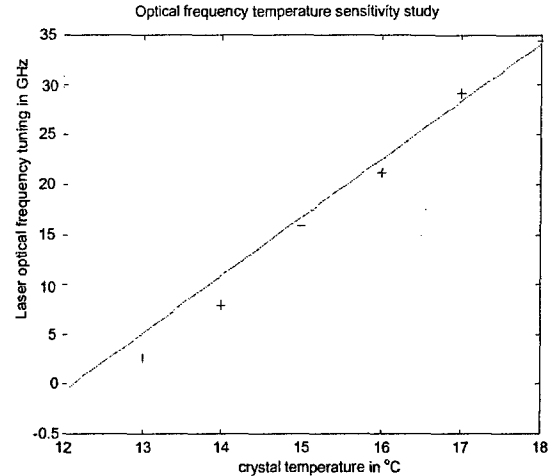


Fig. 13. Optical frequency temperature sensitivity. The optical frequency at 12°C is used as reference [35].

Chirped Heterodyne Transmitter: The experimental setup for the characterization of the chirped heterodyne transmitter is shown in Fig. 15. To generate a chirped signal, an electrical ramp voltage signal is applied to one laser while the other laser sees no electric field. Since the applied electrical field shifts the optical frequency of the laser, a chirped beat frequency is generated in the detector. The electrical voltage tuning is a very fast process, resulting in a fast chirp.

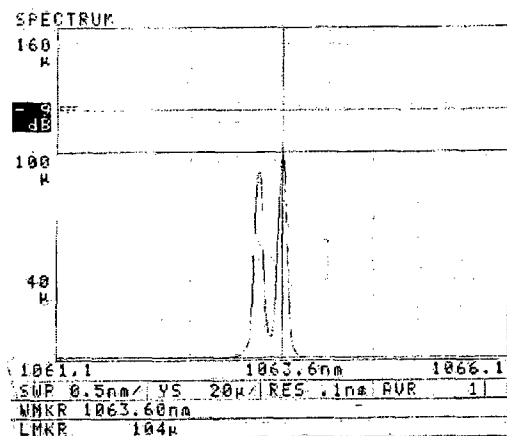


Fig. 14. Optical spectrum of the combined laser outputs. The wavelength separation is 0.3 nm [35].

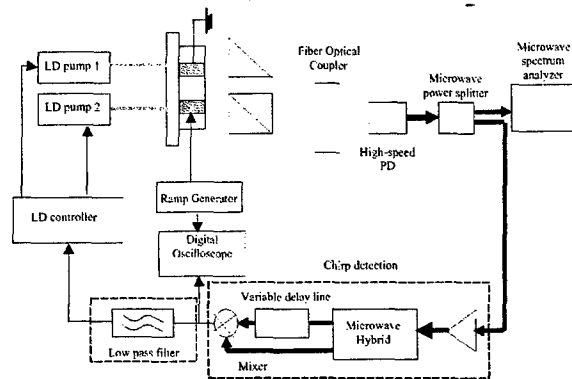


Fig. 15. The transmitter and measurement block diagram [35].

Although the monolithic laser structure provides for stability, fluctuations of the pump power can result in noise in the beat frequency. To obtain a stable signal, a feedback scheme using a microwave homodyne discriminator is introduced. The microwave homodyne discriminator is also used to recover the chirping signal. A low pass filter with stop band of 500 Hz is used to separate the slow random frequency drifting terms and fast tuning voltage induced FM terms. By this way, the feedback only tracks the low frequency drifting and it has not effect to the fast voltage tuning process.

The transmitter was tested with the beat frequency ranging from 7 to 10 GHz. Fig. 16 shows the microwave spectrum with a beat frequency of 7.889GHz. The transmitter electrical tuning sensitivity is characterized by applying 10KHz, 5volt peak-peak ramp tuning signal and measuring the output from microwave homodyne discriminator. The result, shown in Fig. 17, indicates a sensitivity of 8.8MHz/volt.

For the chirping measurement a 1MHz 10 Volt peak-peak ramp signal is applied to one of the lasers. Fig. 18 shows the recovered frequency chirping as well as the applied ramp signal in a sampling oscilloscope. A frequency beat sweep of 88.9 MHz over 0.5 μ s time period was obtained. This corresponds to a 177.8GHz/ms sweeping rate. The frequency chirping resembled the ramp signal except for some distortion due to the system noise.

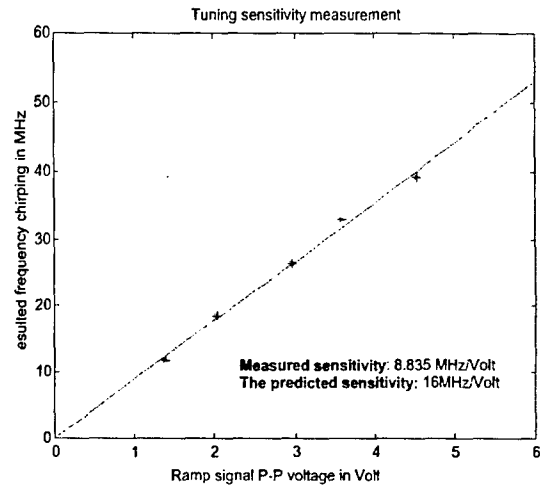
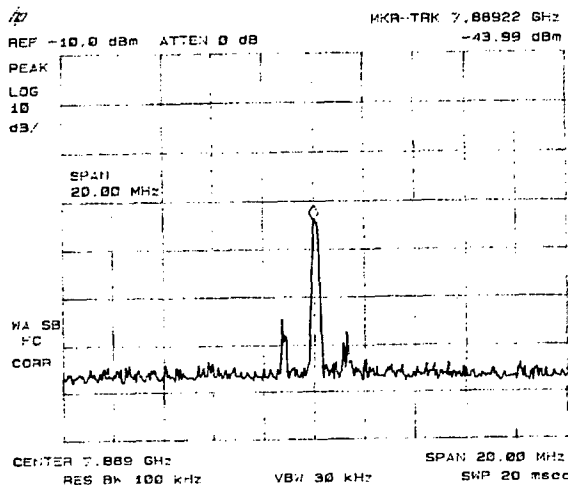


Fig. 16. Microwave spectrum of the beat frequency with no tuning signal [35].

Fig. 17. Transmitter voltage tuning sensitivity [35].

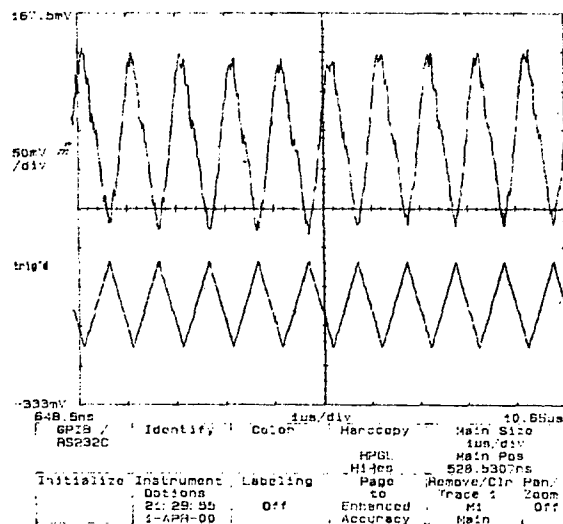


Fig. 18. Measured 1MHz repetition rate 10-volt peak-peak ramp signal modulation response. The upper trace is the recovered frequency-chirping signal. The lower trace is the applied ramp signal [35].

Conclusions

Novel devices are introduced that will lead the microwave photonics applications to a number of future military system applications. Light interaction with microwave devices and circuits will see a new resurgence, particularly in applications dealing with integrated optical detectors with microwave functions as optical clock recovery circuits and multifunction circuits such as optoelectronic mixers. HBT based devices (heterojunction photo transistor) seems to provide high gain and speed performance. Another application of microwave photonics is in development of optical ADC, where various methodologies are considered in achieving high resolution GSPS analog to digital converters. Among these approaches all optical ADC has the greatest promise. An important military application of microwave photonics is the use of photon density waves for medical imaging. The RF modulated light at microwave frequency provides a higher spatial resolution for medical imaging based on the calculated scattering and absorption parameters. The measured results will lead to blood volume of both oxy- and deoxy-hemoglobin, which enable us to develop monitoring systems to assess the pilot overload. Finally, microchip lasers are introduced where a tunable high-speed optical transmitter has been introduced. The transmitter consists of two microchip lasers co-located on the same crystal assembly. The outputs of the two lasers are heterodyned to produce a tunable millimeter wave signal. The composite cavity design provides single mode operation, while maintaining excellent efficiency. The monolithic configuration of realizing two lasers within one microchip crystal makes the transmitter more tolerant to the environmental fluctuations. A novel frequency stabilization scheme is used. The measured tuning sensitivity is around 8.8MHz/Volt. Chirping operation up to 2MHz repetition rate is achieved with good result. Thus we can conclude the tunable optical transmitter provides a good solution to chirped lidar-radar, optical/wireless communications and biomedical imaging.

References

- [1] M. Belaga, *Application of an Optically Controlled PIN Diode in Microwave Circuits*, MS Thesis, Drexel University, Philadelphia, PA, 1987.
- [2] P. Cheung, D.P. Neikirk and T. Itoh, "Optically controled coplanar waveguide phase shifters," *IEEE Trans. on Microwave Theory & Techn.*, Vol.38, No.5, pp.586-595, 1990.
- [3] R. Simons, "Microwave performance of an optically controlled AlGaAs/GaAs high electron mobility transistor and GaAs MESFET," *IEEE Trans. on Microwave Theory & Techn.*, Vol.35, No.12, pp.1444-1455, 1987.
- [4] A. Rosen and F.Zutavern, *High-power Optically Activated Solid-state Switches*, Artech-House Inc., 1994.
- [5] A. S. Daryoush, K. Bontzos and P. R. Herczfeld, "Optically Tuned Patch Antenna for Phased Array Applications," *IEEE International APS Symposium Digest*, Philadelphia, PA, 1986.
- [6] Y. Akatsu, "High-speed monolithically integrated pin-HEMT photoreceivers," *Proceedings of the 1995 IEEE/LEOS Summer Topical Meeting*, ICs for new age lightwave communications, pp.33-34.
- [7] A.L. Gutierrez-Aitken, K. Yang, X. Zhang, G.I. Haddad, P. Bhattacharya and L.M. Lunardi, "16-GHz bandwidth InAlAs-InGaAg monolithically integrated p-i-n/HBT photoreceiver," *IEEE Photon. Tech. Lett.*, Vol.7, No.11, pp.1339-1341, Nov.1995
- [8] S. Chandrasekhar, L. Lunardi, A.H. Ganuck, R.A. Hamm and G.J.Qua, "High-speed monolithic p-i-n/HBT and HPT/HBT photoreceivers implemented with simple phototransistor structure," *IEEE Photon.Tech.Lett.*, Vol.5, No.11, pp.1316-1318, 1993.

- [9] J. Lasri, D. Dahan, A. Bilenca, G. Eisenstein, and D. Ritter, "Clock Recovery at Multiple Bit Rates Using Direct Optical Injection Locking of Self Oscillating InGaAs/InP Heterojunction Bipolar Photo-transistor," *IEEE Photon. Tech. Lett.*, Vol. 13, pp. 1355-1357, 2001.
- [10] A.J. Seeds and A.A.A. de Salles, "Optical control of microwave semiconductor devices," *IEEE Trans. on Microwave Theory & Techn.*, Vol.38, No.5, pp.577-585, 1990.
- [11] A. Madjar, P. Herczfeld and A. Paoella, "A novel analytical model for optically generated currents in GaAs MESFETs," *IEEE Trans. on Microwave Theory & Techn.*, Vol.40, No.8, 1992.
- [12] M.A. Romero, *Modulation doped field effect photodetectors*, Ph.D. Thesis Dissertation, Drexel University, Philadelphia, PA, 1995.
- [13] H. Ogawa, S. Banba, E. Suematsu, H. Kamitsuna and D. Polifko, "A comparison of Noise performance between a pin diode and MMIC HEMT and HBT optical receivers," *the 1993 IEEE International Microwave Symp. Digest*, pp.225-228, Atlanta, GA.
- [14] A. Paoella, A. Madjar and P. Herczfeld, "Modeling the GaAs MESFET's response to modulated light at radio and microwave frequencies," *IEEE Trans. on Microwave Theory & Techn.*, Vol.42, No.7, pp.1122-1130, 1994.
- [15] A.H. Madjedi, S.K. Chaudhuri, and S. Safavi-Naeini, "Optical-Microwave Interaction Modeling in High-temperature Superconducting Film," *IEEE Trans. on Microwave Theory & Techn.*, Vol. 49, No. 10, pp. 1873-1881, 2001.
- [16] B. L. Shoop, *Photonic Analog-to-Digital Conversion*, Springer 2001.
- [17] P.W. Juodawlkis, J.C. Twichell, G.E. Betts, J.J. Hargreaves, R.D. Younger, J.L. Wasserman, F.J. O'Donnell, K.G. Ray, R.C. Williamson, "Optically sampled analog-to-digital converters" *IEEE Trans. Microwave Theory & Techn.*, Vol. 49, No. 10, pp. 1840 -1853, Oct. 2001.
- [18] T.R. Clark, J.U. Kang, R.D. Esman, "Performance of a time- and wavelength-interleaved photonic sampler for analog-digital conversion," *IEEE Photon. Tech. Lett.*, Vol. 11, No. 9, pp.1168 -1170, Sept. 1999.
- [19] A. S. Bhushan, P. V. Kelkar, B. Jalali, O. Boyraz and M. Islam, "130-Gsa/s Photonic Analog-to-Digital Converter with Time Stretch Preprocessor", *IEEE Photonic Technology Letters*, Vol. 14, No. 5, May 2002, pp684-686
- [20] H. F. Taylor, "Electro-Optic A/D Converter, US patent 4058722
- [21] B. Jalali and Y. M. Xie, " Optical folding-flash analog-to-digital converter with analog encoding", *Opt. Lett.*, Vol. 20, No. 18, pp1901-1903, 1995.
- [22] M. J. Hayduk, "Photonic Analog-to-Digital Conversion Using Light Absorption" US patent # 6326910.
- [23] J. T. Gallo, "Photonic A/D converter using parallel synchronous quantization of optical signals", US patent # 6188342.
- [24] H. Zmuda, E.N. Toughlian, G. Li, P. Li Kam Wa, "A photonic wideband analog-to-digital converter", *Proceedings of the 2001 IEEE Aerospace Conference*, Vol. 3, pp. 1461 -1472.
- [25] B. Chance, M. Cope, E. Gratton, N. Ramanujam, B. Tromberg, "Phase measurement of light absorption and scatter in human tissue," *Rev. of Sci. Inst.* 69, 3457-3481 (1998).
- [26] B. Tromberg, N. Shah, R. Lanning, A. Cerussi, J. Espinoza, T. Pham, L. Svaasand, and J. Butler, "Non-Invasive In vivo Characterization of Breast Tumors Using Photon Migration Spectroscopy," *Neoplasia* 2, 26-40 (2000).
- [27] J.B. Fishkin, O. Coquoz, E. Anderson, M. Brenner, and B. Tromberg, "Frequency-domain photon migration measurements of normal and malignant tissue optical properties in a human subject," *Appl. Opt.* 36, 10-20 (1997).
- [28] B. Chance, E. Anday, S. Nioka, S. Zhou, L. Hong, K. Worden, C. Li, T. Murray, Y. Ovetsky, D. Pidikiti, and R. Thomas, "A novel method for fast imaging a brain function, non-invasively, with light," *Opt. Express*, 2, pp. 311-423.
- [29] V. Ntziachristos, A.G. Yodh, M. Shnall, and B. Chance, "MRI-guided diffuse optical spectroscopy of malignant and benign breast lesions," *Neoplasia* (in press).
- [30] J.B. Fishkin, and E. Gratton, "Propagation of photon density waves in strongly scattering media containing an absorbing semi-infinite plane bounded by a straight edge." *J. Opt. Soc. Am.*, A 10, pp. 127-140 (1993).

- [31] Fantini S, Franceshini M, and Gratton E, "Semi-infinite-geometry boundary problem for light migration in highly scattering media: a frequency-domain study in the diffusion approximation," *J. Opt. Soc. Am.*, B 11, pp. 2128-2138 (1994).
- [32] J.B. Fishkin, S. Fantini, M.J. vandeVen, and E. Gratton, "Gigahertz photon density waves in a turbid medium: Theory and experiments," *Phys. Rev.*, E 53, P. 2307 (1996).
- [33] T.H. Pham, O. Coquoz, J.B. Fishkin, E. Anderson, and B. Tromberg, "Broad bandwidth frequency domain instrument for quantitative tissue optical spectroscopy," *Rev. Sci. Inst.* 71, 2500-2513(2000).
- [34] G.J. Simonis and K.G. Purchase, "Optical Generation, Distribution, and Control of Microwaves Using Laser Heterodyne", *IEEE Trans. Microwave Theory & Techn.*, Vol. 38, No. 5, pp. 667-669, May 1990.
- [35] Y. Li, A.J.C. Vieira, P. Herczfeld, A. Rosen, W. Janton, "Rapidly tunable millimeter-wave Optical transmitter for Lidar-Radar", *IEEE Trans. Microwave Theory & Techn.*, Vol. 49, No. 10, October 2001.